Journal of Materials Chemistry A

Accepted Manuscript

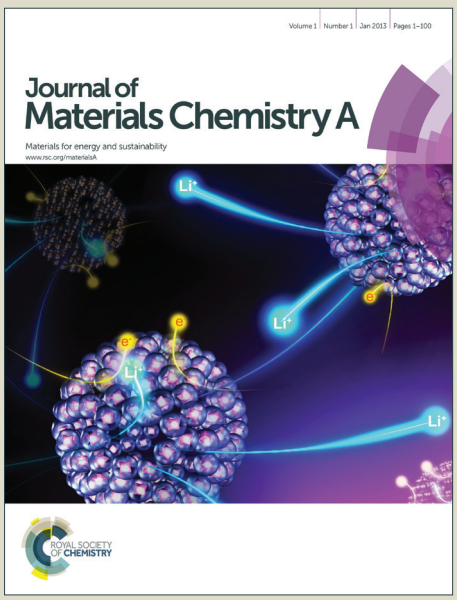

ROYAL SOCIETY OF CHEMISTRY

www.rsc.org/materialsA

Cite this: DOI: 10.1039/c0xx00000x

www.rsc.org/xxxxxx

ARTICLE TYPE

MOFs derived catalysts for electrochemical oxygen reduction

Xiaojuan Wang,[a] Junwen Zhou,[a] He Fu,[a] Wei Li,[a] Xinxin Fan,[a] Gongbiao Xin,[a] Jie Zheng, *[a] and Xingguo Li*[a]

Received (in XXX, XXX) Xth XXXXXXXXX 20XX, Accepted Xth XXXXXXXXX 20XX

DOI: 10.1039/b000000x

To develop noble metal free catalysts for the oxygen reduction reaction (ORR) is of critical importance for the production of low cost polymer electrolyte membrane fuel cells. In this paper, metal organic frameworks (MOFs) are used as precursors to derive ORR catalysts via pyrolysis in inert atmosphere. The ORR performance is found to be closely associated with the metal/ligand combination in the MOFs. The Co-imidazole based MOF (ZIF-67) derived catalyst exhibits the best ORR activity in both alkaline and acidic electrolytes. The Co cations coordinated by the aromatic nitrogen ligands in ZIF-67 may assist the formation of the ORR active sites in the derived catalyst. The best ORR performance is obtained when the porosity of the derived catalyst is maximized, by optimizing the pyrolysis temperature and the acid leaching process. The performance of the best MOF derived catalyst is comparable to that of Pt/C in both alkaline and acidic electrolytes.

Introduction

The electrochemical reduction of oxygen (known as the oxygen reduction reaction, ORR) is the cathode reaction in fuel cells. Due to the sluggish kinetics of ORR, high loading of Pt catalysts is required to accelerate the ORR in polymer electrolyte membrane fuel cells (PEMFCs). Even with the state-of-the-art technology, the Pt loading for ORR is still 5-10 times higher than that in the anode[1]. To realize large scale application of PEMFC, the Pt loading should be substantially reduced while maintaining the same catalytic activity or, more attractively, be replaced by low cost, noble metal free catalysts.

Noble metal free catalysts based on non-precious transition metals, such as Fe[2, 3]and Co[4-6] and/or N doped carbon materials[7, 8], are extensively investigated. Previous studies suggest that both the transition metals and the N dopant are important to achieve high ORR activity. A proposed ORR active site based on transition metals is the porphyrin-like MN_x (M=Fe or Co) structure[9-13]. In N-doped carbon nanostructures, the incorporated N with the adjacent C atoms may serve as metal-free ORR centres[14, 15]. Although transition metals do not directly appear, they are either involved during the preparation process[16] or may further enhance the ORR performance[17]. In addition, the ORR performance also depends on the density of the active sites and how these active sites are distributed in the electrode material. As a result, formation of active sites with high density and proper assembly of the metal, N and C components is critical to achieve high ORR performance. However, this process can be rather challenging and sophisticated, particularly when starting from individual components[18, 19]. Attractively, Fe, Co complexes with N-coordinated ligands, such phthalocyanine[20], terpyridine[21] and phenanthroline[22] , often exhibit prominent ORR performance after controlled heat treatment. Since the N-coordinated metal centres in these precursors may assist the formation of the active ORR sites, this inspires us to further explore materials with well-organized assembly of the metal, N and C components as precursors to derive ORR catalysts.

Metal organic frameworks (MOFs) are highly ordered 3D framework structures composed of well-organized metal centres and organic linkers. In addition to their extensively studied applications based on the porosity (e.g. gas storage and separation[23-25]), there is increasing interest in deriving functional nanostructures by using MOFs as precursors[26-29]. One of the beneficial features for catalysis through this protocol is that the metal centres in MOFs are located in well-defined coordination environment, viable for rational design and systematic improvement. Though there have been a few pioneered works on MOF-derived ORR catalysts with promising performances[10, 30-35], only very limited structures in the large MOF family have been studied. A key issue determining the ORR performance of the derived catalysts is the metal/ligand combination in the MOF structure. However, current work is almost limited to a few MOFs. The effect of the metal/ligand combination remains to be clarified. Moreover, the processing conditions also strongly affect the ORR performance. To optimize the processing conditions, it is necessary to understand the structural change of the MOFs during the processing. This issue, however, has not been studied in detail.

In this paper, we study the ORR catalysts derived from three MOFs with representative structures to illustrate the critical role of the metal/ligand combination in the MOF structure. The combination of Co metal and the 2-methylimidazole ligand is found to give the best ORR performance after pyrolysis. The metal coordination environment in this MOF structure mimics the

proposed active ORR sites CoN_x, which suggests that the well-defined chemical environment of the metal centres in MOF structures can be utilized to derive ORR catalysts with high performance. Meanwhile, we demonstrate that both rich nanoporosity and ordered graphitic structure are beneficial for ORR, which provides guidelines for the processing optimization.

Experimental section

Three representative MOF structures are investigated as the precursors: 1) ZIF-67 ($Co(MeIM)_2$, MeIM=2-methylimidazole), with four-fold coordinated Co atoms bridged by MeIM linkers, 2) ZIF-8, the Zn analogy of ZIF-67 and 3) $Co_2(bdc)_2(dabco)$ (bdc = 1,4-benzenedicarboxylate;dabco = 1,4-diazabicyclo[2.2.2]octane) in which Co atoms are coordinated by one N atom from dabco and four O atoms from bdc. The crystal structures of these MOFs are illustrated in supporting information (Fig. S1). Such choices allow us to study how the metal/ligand combination will affect the ORR performance.

These MOFs are prepared based on well established procedures in literature[28, 36] (see also supporting information). The ORR catalysts are prepared by temperature programmed pyrolysis of the MOFs in Ar atmosphere. Typically, 0.5 g MOF is heated to 600-1000 ^oC at 10 ^oC min^{-1} under an Ar stream in a tube furnace, then kept at the peak temperature for 10 min and allowed to cool down to room temperature. The samples are designated by MOF-T, where T is the carbonization temperature, or MOF-T-AL if acid leaching is employed. Details of the preparation methods, structural characterization and electrochemical measurements are in the supporting information.

Results and discussion

Table 1 Element compositions (in wt%) and specific surface area (S_{BET}) of the MOFs derived ORR catalyst samples

Sample	N	C	H	Metal	S_{BET} (m^2g^{-1})
ZIF-67-600	10.9	38.3	1.4	34.4	32.98
ZIF-67-700	6.9	41.1	1.0	37.4	258.2
ZIF-67-800	4.7	44.1	0.8	40.4	303.5
ZIF-67-900	4.0	48.8	0.5	38.3	285.9
ZIF-67-900-AL	1.4	93.1	0.3	4.7	501.7
$Co_2(bdc)_2(dabco)$-900	0.3	36.2	1.0	51.0	182.8
ZIF-8-900	5.5	66.2	2.5	7.9	883.5

Table 1 summarizes the composition analysis results of the MOF-derived catalysts. The products are composed of C, N and the metal in the parent MOF. The ZIF-8-900 sample shows much lower metal content compared with the two Co based samples, which is attributed to the high volatility of Zn at the carbonization temperature. The two ZIFs give comparable N/C ratio around 1/12 after heat treatment at 900 ^oC. The higher absolute N percentage in the ZIF-8-900 sample is owing to the lower metal content. However, the $Co_2(bdc)_2(dabco)$-900 sample only contains 0.3 wt% N, significantly less than the two ZIF-derived catalysts. The above results suggest that the nature of the N in the MOF precursor has significant impact on the amount of N incorporated in the resulting catalyst. Aromatic N is more inclined to be incorporated into the carbon skeleton after carbonization than aliphatic N. This is easy to understand since the N atoms in the aromatic rings are more strongly bonded with carbon. X-ray diffraction patterns (Fig. S3) indicate that all the three pyrolyzed samples are composed of the pure metallic phase of the metal in the parent MOF. The two Co based catalysts and ZIF-8-900 exhibit the face-centred cubic Co phase and the hexagonal Zn phase, respectively.

The two Co based catalysts have similar morphology, as suggested by the transmission electron microscopy (TEM) results (Fig. 1). Both catalysts are composed of Co nanoparticles around 5-15 nm embedded in the carbon matrix (Fig. 1a and 1c, Fig. S4a). The Co particles exhibit well resolved {111} lattice fringes with interspacing of 0.204 nm (Fig. 1b, inset). The Co particles are formed upon the collapse of MOF during the pyrolysis process followed by aggregation of the metal species (individual ions and small particles). Migration of the metal species leaves voids in their original position, as indicated by the arrow in Fig. 1b. Clear graphitic layers can be observed around the Co particles (Fig 1b. and Fig. S4a). Formation of such graphitic layers is resulted from the catalytic effect of Co, as such layer structure is not observed in the ZIF-8 derived catalyst (Fig. S4b).For ZIF-8-900, metal particles are rarely observed, which is in agreement with the low Zn content. As shown in Fig. 1d and Fig. S4b, the sample also shows a porous structure. The porosity here is originated from the high volatility of Zn at the pyrolysis temperature. In fact, pyrolysis of ZIF-8 has been utilized to prepare porous carbon materials with ultrahigh surface areas[26]. For this reason, the ZIF-8-900 sample shows a much higher BET surface area compared with the two Co-based catalysts (Table 1, Fig. S5).

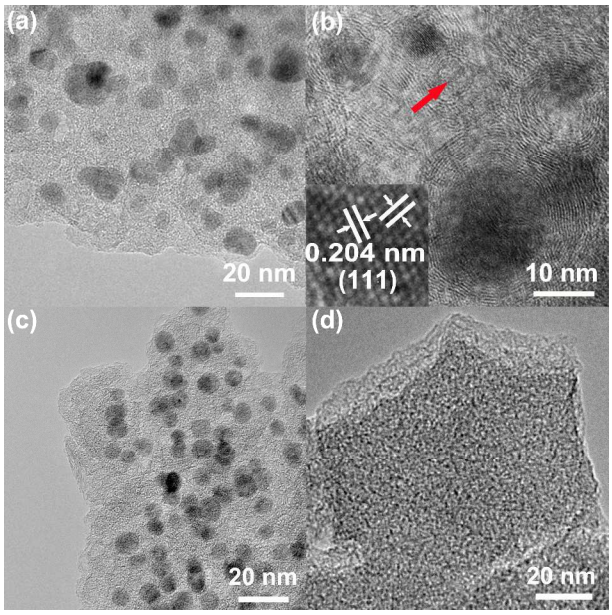

Fig. 1. TEM images of MOF derived catalysts: (a-b) ZIF-67-900, (c) $Co_2(bdc)_2(dabco)$-900, (d) ZIF-8-900. The arrow in (b) indicates a void enclosed by graphitic layers. The inset in (b) is a lattice image of a Co particle.

As a brief summary, the two Co based catalysts exhibit very similar structure, i.e. fine Co nanoparticles embedded in graphitized carbon, but with very different N content. The two ZIF-derived catalysts are very similar in their N/C ratio, while the ZIF-8-900 sample shows much lower metal content compared with its Co counterpart.

The ORR performance of the three MOF derived catalysts is measured by linear scanning polarization curves on a rotating disk electrode (RDE) in both alkaline (O_2-saturated 0.1 M KOH solution) and acidic (0.5 M H_2SO_4 solution) electrolytes, respectively. The results of the commercial Pt/C catalysts with 10% Pt loading are also shown for comparison. The negative current is attributed to the reduction of oxygen, which is confirmed by the comparative cyclic voltammogram measurements in O_2-saturated and O_2-depleted solutions (Fig. S12).

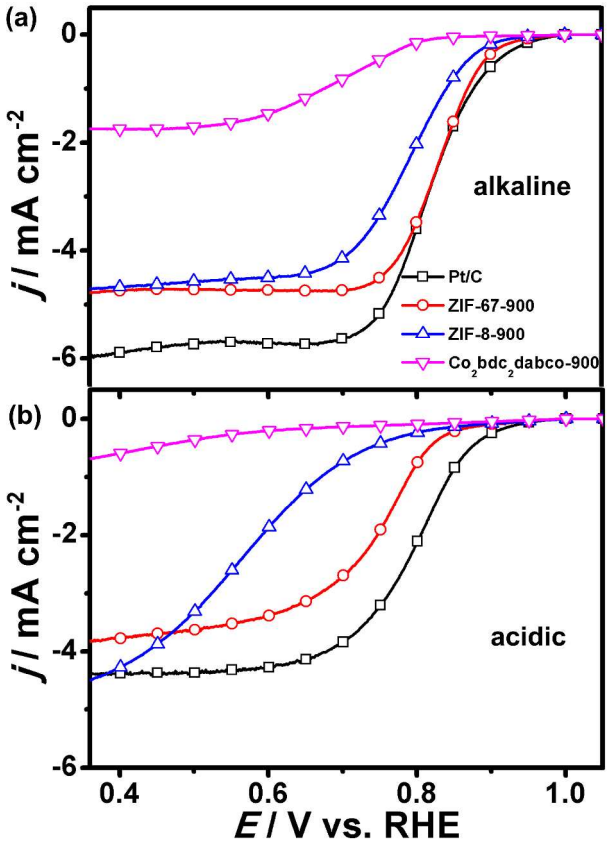

Fig. 2 Linear scanning polarization curves (scan rate of 10 mV s^{-1}) of different MOF-derived catalysts and Pt/C (10 wt%) recorded in O_2-saturated 0.1 M KOH solution (a) and 0.5 M H_2SO_4 solution (0.1 M $HClO_4$ for Pt/C) (b). The measurements are carried out on a rotating disk electrode a rotating rate of 1600 rpm.

In the alkaline electrolyte, the two ZIF-derived catalysts exhibit very high catalytic performance (Fig. 2a). The ZIF-67-900 sample shows an onset potential of 0.91 V and a halfwave potential of 0.85 V, very close to that of Pt/C (0.92V for onset and 0.84 V for halfwave potential). The ZIF-8-900 sample shows slightly more negative onset potential (0.89 V) and halfwave potential (0.82 V). Both samples show comparable saturated current density (~5 mA·cm^{-2}), about 83% of that of Pt/C. The catalytic performance of $Co_2(bdc)_2$dabco-900 sample, however, is much inferior. A very negative onset potential 0.82 V is observed, which means a large overpotential when used in fuel cells. The saturated current density is also very low (lower than 2 mA·cm^{-2}). In the acidic electrolyte, the $Co_2(bdc)_2$dabco-900 sample barely shows any catalytic effect: only a very low current density (< 1 mA·cm^{-2}) is obtained in very negative potential (0.30 V). Interestingly, the difference between two ZIF derived catalysts becomes prominent. The polarization curve of the ZIF-8-900 sample starts to deviate from that of Pt/C, showing more negative onset and halfwave potential. The ZIF-67-900 sample, impressively, still shows high ORR activity. The onset potential (0.85 V) and halfwave potential (0.71 V) is only a bit more negative than that of Pt/C.

The distinct ORR activities of the two Co based catalysts are particularly illuminating for the critical role of N doping, since they are very similar in phase composition, particle size and carbon morphology, except for the N content. The chemical bonding nature of the N species in the catalysts are studied in detail with X-ray photoelectron spectroscopy (XPS, Fig. S6b). Two characteristic peaks corresponding to pyrrolic (400.5 eV) and pyridinic (398.3 eV) N can be resolved, with a shoulder at 402 eV corresponding to the graphitic N. The spectrum of $Co_2(bdc)_2$dabco-900 is quite noisy due to the low N content. The two characteristic peaks can still be observed. Both the pyrrolic and pyridinic N have been identified to have ORR activity[37, 38]. The low activity of the $Co_2(bdc)_2$dabco-900 sample, therefore, can be explained by its low nitrogen content.

On the other hand, the superior performance of ZIF-67-900 over that of ZIF-8-900 further implies that the transition metal also plays an important role. Our study suggests that compared with Zn, a valuable advantage of Co is that it remains considerable activity for ORR catalysts in acidic electrolyte. Indeed, Co has long been recognized to be a component for ORR active sites in both acidic and alkaline electrolyte[4, 16]; Zn based ORR catalysts are rarely reported. Zhang et al. have used Zn based ZIFs as the pyrolysis precursor to derive high performance ORR catalysts[35]; however, the performance in acidic electrolyte was not reported. Instead, to achieve high performance in acidic electrolyte, iron species has to be included in the MOF structure to yield the catalytic sites[30, 34].

As suggested by previous studies, the possible ORR active sites here can be the N-coordinated Co structures CoN_x, which has similar local chemical environment to the Co-porphyrin structure. EXAFS[31, 39, 40] or Mössbauer spectroscopy studies[32, 41] have suggested similar structure in Co based ORR catalysts. One indirect evidence is the predominance of the pyrrolic and pyridinic N atoms, i.e. N atoms located on the edge of the graphitic sheets which can serve as coordination sites with the metal ions.

Here formation of the active sites is strongly related to the coordination environment of the metal cations in the parent MOF structure. The superior performance of ZIF-67-900, therefore, is not surprising: the well-defined four-fold N-coordinated Co atoms are ideal precursors to achieve this Co-N synergy (Fig. S1). Moreover, the aromatic nature of the N in the ligand also plays an essential role, as reflected by the different performances of the two Co based catalysts. N atoms in the aromatic rings, stronger bonding to the carbon skeleton, are more likely to remain in the resulting carbon backbone after pyrolysis. Our comparative study provides a guideline for the choice of the metal/ligand combination: transition metals like Fe or Co paired with ligands containing aromatic N.

The performance of the ZIF-67 derived catalysts is further optimized. The pyrolysis temperature is found to have a strong

effect on the ORR performance. As shown in Fig.3, higher pyrolysis temperature results in better ORR activity in both acidic and alkaline electrolytes, characterized by positive shifts of both the onset and halfwave potentials as well as enhanced saturation current densities. Surprisingly, the difference in microstructures among samples with different pyrolysis temperatures are not significant, as suggested by XRD and TEM (See Table 1, Fig. 1b, S8 and S9): Co nanoparticles with sub-15nm in size are all well distributed and embedded in N-doped graphitic carbon matrix. It is therefore very intriguing to study how the slight difference in microstructures could lead to such distinct catalytic properties.

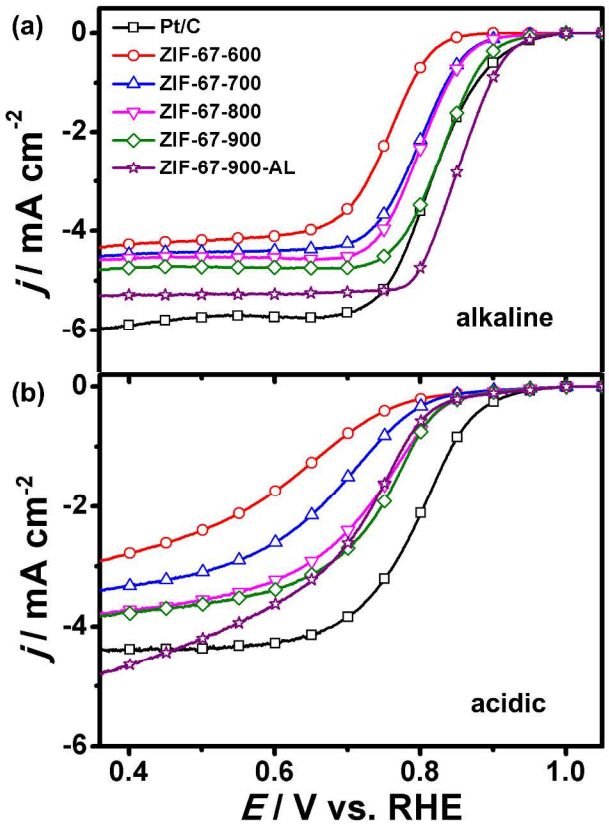

Fig. 3 Linear scan polarization curves of the ZIF-67-T samples and the acid leached sample ZIF-67-900-AL in O_2- saturated 0.1 M KOH (a) and 0.5 M H_2SO_4 (0.1 M $HClO_4$ for Pt/C) (b), measured on a RDE at 1600 rpm with the scan rate of 10 mV s^{-1}.

As the ORR activity comes from the synergy of Co and N, we first consider the temperature effect on these two components. N content decreases with increasing pyrolysis temperature (Table 1), as some volatile N containing species would escape at elevated temperature. There is also a slight increase of the pyrrolic N/pyridinic N ratio at higher temperature (Fig. S10b). For the Co component, higher pyrolysis temperature causes aggregation of the Co particles (Fig. 1b and S9). XPS spectra (Fig. S10a) suggest that the ZIF-67-T samples contain both metallic (778.3 eV) and divalent (780.4 eV) Co. The divalent Co comes from the surface Co atoms that may have interaction with the carbon matrix, which also includes the proposed active sites CoN_x. Higher pyrolysis temperature increases the metallic fraction. This is consistent with the larger Co particle size obtained at higher temperature, as larger particles have smaller surface/bulk ratio. Therefore, in terms of the two components for the proposed active site CoN_x, higher pyrolysis temperature seems to reduce the density of the CoN_x sites and is not favourable for ORR activity.

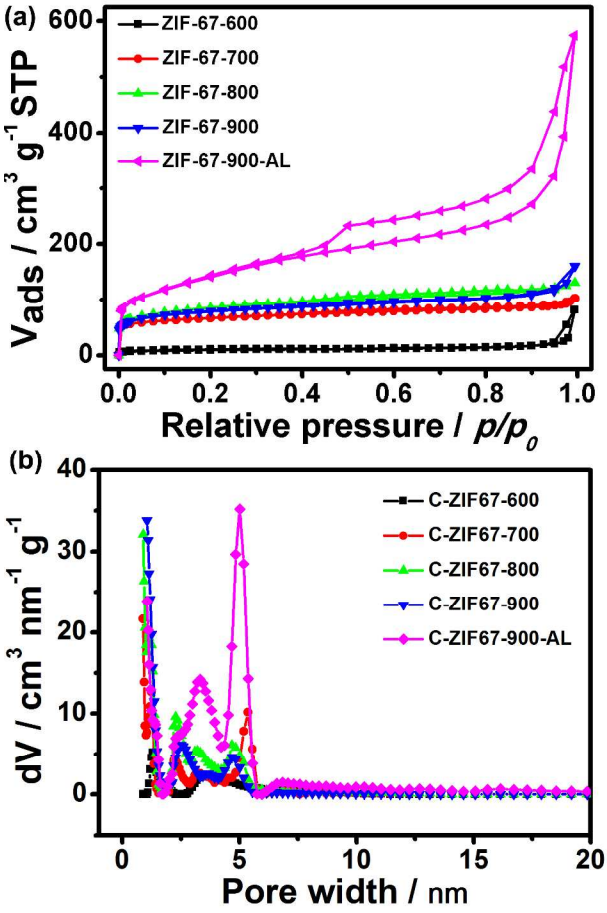

Fig. 4 N_2 adsorption isotherms (a) and pore size distribution (b) of ZIF-67 derived catalysts.

A next factor in consideration is the different porosities of the catalysts. Fig. 4 shows the N_2 adsorption isotherms and the corresponding pore size distributions of the ZIF-67 derived catalysts. ZIF-67-600 is almost non-porous with a low surface area of 33 m^2/g. A pyrolysis temperature higher than 700 °C significantly increases specific surface areas and porosity (Table 1), which, as mentioned above, is resulted from the migration of the small Co particles, leaving nanoscale voids in the original position. Such voids enclosed by graphitic carbon layers can be clearly observed in TEM images (Fig. 1b, Fig. S9). Nanoscale pores are considered to be favourable for the ORR.[37,42] Therefore, the general trend that the ORR performance is improved with the pyrolysis temperature can be explained by the enhanced surface area and porosity.

However, there remains a small inconsistence. ZIF-67-900 shows better ORR performance than ZIF-67-800, albeit with lower surface area and pore volume. To explain this, the difference in the carbon structure need to be taken into account. Fig. S11 shows the Raman spectra of the ZIF-67-T samples. The G band at ~1590 cm^{-1} and the D band at ~1330 cm^{-1} can be clearly resolved. In addition, the low T samples exhibit another two features at ~1180 and ~1470 cm^{-1}, which are referred to the I

band and the D'' band, respectively. Both the I and the D" bands have been observed in the Raman spectra of N-doped carbon nanotubes.[43, 44] The broad I band is related to the N or other impurities in the graphitic structure[44]. The D'' band is an indicator to the stacking disorder of the graphene layers[43]. As shown in Fig. 5, the integrated band ratios I_D/I_G is almost unchanged with pyrolysis temperature, in agreement with the TEM results where clear graphitic layers can be observed for all the ZIF-67-T samples. However the ratio $I_{D''}/I_G$ shows a clear decrease trend with the pyrolysis temperature, indicating that higher pyrolysis temperature leads to a more ordered graphitic structure. This is in consistence with the lower N content (Table 1), since the incorporated N is a major source of disorder in the graphitic structure. The more ordered graphitic structure improves the electrical conductivity of the catalysts (Table S1). This effect compensates the slightly lower surface area and porosity and explains the improved performance of ZIF-67-900 compared to that of ZIF-67-800.

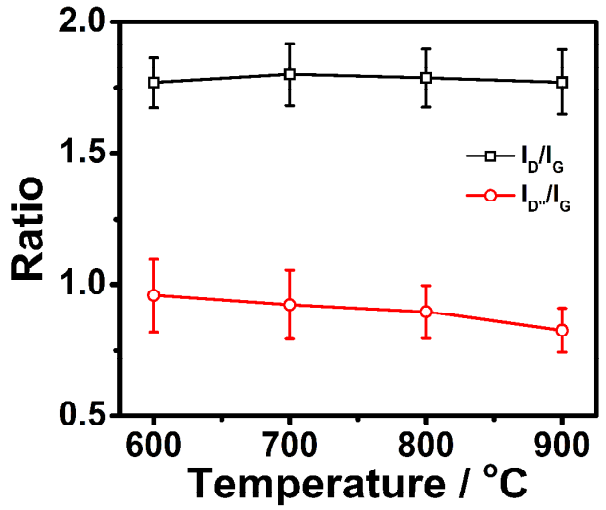

Fig. 5. The integrated band ratio I_D/I_G and $I_{D''}/I_G$ from the Raman spectra for the ZIF-67-T samples obtained at different pyrolysis temperature.

The structure evolution of ZIF-67 during the carbonization process is schematically illustrated in Fig. 6. The framework starts to collapse at around 400 °C (Fig. S7), yielding tiny Co nanoparticles around 5 nm embedded in a carbon matrix (Fig. S9a). At higher temperatures, the small Co nanoparticles start to aggregate and leave voids in their original location, resulting in a nanoporous structure (Fig. 1b). Co atoms with stronger interaction with the carbon matrix, for instance, those directly bonding with the pyrrolic/pyridinic N, are retained in the nanosized voids. These N-coordinated Co sites inside the nanoscale pores serve as the active ORR sites.

This picture thus provides guidelines to further enhance the ORR activity. We note that the ZIF-67-900 sample contain up to 30 wt% Co. The Co particles occupy the nanopores and block the active sites. Removing these excessive Co particles, by acid leaching for instance, can expose more CoN_x sites.

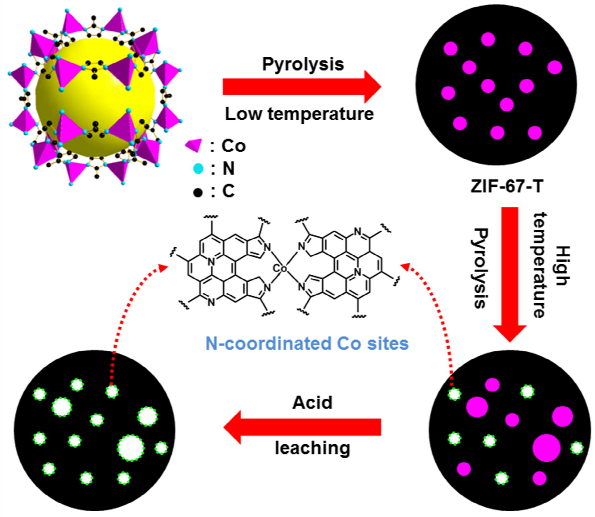

Fig. 6. Schematic illustration of the synthesis process for the ZIF-67-T catalysts. The coordination environment of Co in the product (a proposed structure) is also shown.

Acid leaching has been extensively used in literature to remove the unstable impurities, which is typically carried out in 0.5-2 M H_2SO_4 at 80 °C [10, 16, 45, 46]. Due to the exceptional high stability of the Co particles enclosed by the graphite layers, we employ much harsher conditions: hydrothermally etching in 10 M HCl at 180 °C for 24 h, followed by heating the resulted solids at 900 °C for 1 h. This process is repeated until the supernatant after the hydrothermal process shows no visible pink colour of Co^{2+}. With this effort, Co content is reduced to 4.7 wt% and the Co particles are almost invisible for the acid leached sample (Fig. 7), producing high density nanosized voids enclosed by graphite layers. Specific surface area almost doubles after the acid treatment (Table 1).

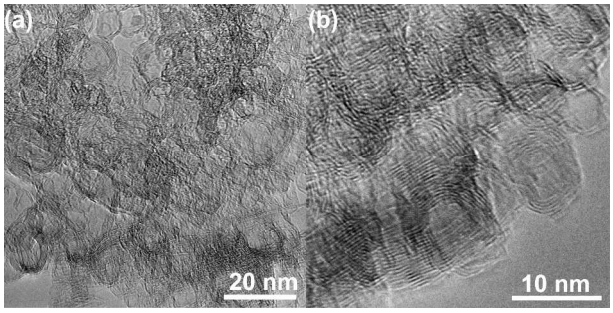

Fig. 7 TEM images of the ZIF-67-900 sample after acid leach.

As predicted, the acid leaching step indeed improves the ORR performance (Fig. 3). The saturate current density is significantly improved in both acid and alkaline electrolyte. There is a further positive shift of the onset and halfwave potentials in alkaline electrolyte. The ORR on the ZIF-67-900-AL sample is a four-electron dominant process in both alkaline and acidic electrolyte (Table S2), as indicated by the rotating ring-disk electrode measurement (Fig. S14) and the Koutecky-Levich plot (Fig. S15 and S16). These improvements are consistent with the picture that acid leaching increases the density of exposed CoN_x sites. Notably, the acid leached sample exhibits even more positive onset and half wave potential than that of Pt/C in the alkaline electrolytes. This is particularly exceptional for noble metal free

ORR catalysts. The sample also exhibits both better stability and tolerance to methanol crossover than the Pt/C catalyst (Fig. S17). The overall performance of the acid leached sample is among the best of the contemporary noble metal free ORR catalysts in both alkaline and acidic electrolyte[11, 16, 30]. A comparison with the state-of-the-art Co based ORR catalysts is shown in supporting information (Table S3)

It is noteworthy that the above Co removal process also reduces the N content to 1.4 wt% (Table 1). The remaining N shows predominant pyrrolic nature (Fig. S10b), which seems to suggest that pyrrolic N is the more stable form. It thus implies that the ORR performance cannot be directly linked with the absolute amount of Co and N. The exact amount of Co and N required for the active sites can be very low; increasing the Co and N content will not necessarily result in more active sites unless the CoN_x sites are accessible. Therefore, the nanoporous structure is strongly desirable to achieve high ORR activity. An ideal structure would be such that the active sites (e.g. CoN_x) are homogeneously distributed on the walls of the open nanopores. Such structure, nevertheless, is difficult to achieve synthetically. In our case, the pores in the ZIF-67-900-AL sample are templated from the removal of Co nanoparticles, which, together with the incorporated N, give birth to high density CoN_x sites inside the nanopores.

Conclusions

In conclusion, we have obtained high performance ORR catalysts by controlled pyrolysis of ZIF-67, a MOF composed of Co and aromatic N-contained ligands. The catalysts exhibit more positive onset and halfwave potentials as well as higher saturation current density than commercial Pt/C catalysts in alkaline electrolytes, and comparable saturation current density in acidic electrolytes. In addition they have better stability and tolerance to methanol crossover in both alkaline and acidic electrolytes. Such high activity is attributed to the highly dispersed active CoN_x sites in the nanoporous conductive system. MOFs, due to their highly ordered coordination environment of metal ions, provide great versatility in creating active sites for catalysis. Clearly, this advantage is not limited to derive catalysts for ORR and deserves more research attention.

The work is supported by MOST of China (No. 2010CB631301) and NSFC (No. 21101007, U1201241 and 11375020).

Notes and references

[a] *Beijing National Laboratory for Molecular Sciences (BNLMS), (The State Key Laboratory of Rare Earth Materials Chemistry and Applications), College of Chemistry and Molecular Engineering, Peking University, Beijing 100871, China.*
Email : xgli@pku.edu.cn; zhengjie@pku.edu.cn

† Electronic Supplementary Information available: detailed experiment and characterization methods; XRD patterns, nitrogen adsorption-desorption isotherms, pore size distributions, and high resolution Co $2p_{3/2}$ and N 1s XPS of MOF-T. RDE tests, CVs and chronoamperometric responses of ZIF-67-900 in alkaline and acidic medium for ORR. See DOI: 10.1039/b000000x/

1. Z. W. Chen, D. Higgins, A. P. Yu, L. Zhang and J. J. Zhang, *Energy & Environ. Sci.*, 2011, **4**, 3167-3192.
2. Z.-S. Wu, S. Yang, Y. Sun, K. Parvez, X. Feng and K. Muellen, *J. Am. Chem. Soc.*, 2012, **134**, 9082-9085.
3. Z. Wen, S. Ci, F. Zhang, X. Feng, S. Cui, S. Mao, S. Luo, Z. He and J. Chen, *Adv. Mater.*, 2012, **24**, 1399-1404.
4. Y. Y. Liang, Y. G. Li, H. L. Wang, J. G. Zhou, J. Wang, T. Regier and H. J. Dai, *Nat. Mater.*, 2011, **10**, 780-786.
5. Y. Y. Liang, H. L. Wang, P. Diao, W. Chang, G. S. Hong, Y. G. Li, M. Gong, L. M. Xie, J. G. Zhou, J. Wang, T. Z. Regier, F. Wei and H. J. Dai, *J. Am. Chem. Soc.*, 2012, **134**, 15849-15857.
6. J. B. Xu, P. Gao and T. S. Zhao, *Energy & Environ. Sci.*, 2012, **5**, 5333-5339.
7. P. Chen, T.-Y. Xiao, Y.-H. Qian, S.-S. Li and S.-H. Yu, *Adv. Mater.*, 2013, **25**, 3192-3196.
8. R. Silva, J. Al-Sharab and T. Asefa, *Angew. Chem. Int. Ed.*, 2012, **51**, 7171-7175.
9. B. Wang, *J. Power Sources*, 2005, **152**, 1-15.
10. D. Zhao, J.-L. Shui, C. Chen, X. Chen, B. M. Reprogle, D. Wang and D.-J. Liu, *Chemical Science*, 2012, **3**, 3200-3205.
11. R. L. Liu, C. von Malotki, L. Arnold, N. Koshino, H. Higashimura, M. Baumgarten and K. Mullen, *J. Am. Chem. Soc.*, 2011, **133**, 10372-10375.
12. H. Tang, H. Yin, J. Wang, N. Yang, D. Wang and Z. Tang, *Angewandte Chemie (International ed. in English)*, 2013, **52**, 5585-5589.
13. M. Jahan, Q. L. Bao and K. P. Loh, *J. Am. Chem. Soc.*, 2012, **134**, 6707-6713.
14. K. P. Gong, F. Du, Z. H. Xia, M. Durstock and L. M. Dai, *Science*, 2009, **323**, 760-764.
15. L. T. Qu, Y. Liu, J. B. Baek and L. M. Dai, *ACS Nano*, 2010, **4**, 1321-1326.
16. G. Wu, K. L. More, C. M. Johnston and P. Zelenay, *Science*, 2011, **332**, 443-447.
17. K. Parvez, S. Yang, Y. Hernandez, A. Winter, A. Turchanin, X. Feng and K. Mullen, *ACS Nano*, 2012, **6**, 9541-9550.
18. F. Jaouen, E. Proietti, M. Lefevre, R. Chenitz, J.-P. Dodelet, G. Wu, H. T. Chung, C. M. Johnston and P. Zelenay, *Energy & Environ. Sci.*, 2011, **4**, 114-130.
19. R. Liu, C. von Malotki, L. Arnold, N. Koshino, H. Higashimura, M. Baumgarten and K. Muellen, *J. Am. Chem. Soc.*, 2011, **133**, 10372-10375.
20. W. M. Li, A. P. Yu, D. C. Higgins, B. G. Llanos and Z. W. Chen, *J. Am. Chem. Soc.*, 2010, **132**, 17056-17058.
21. W. Jiatang, L. Shang, Z. Guangwen, Z. Wei, C. Ruixin and P. Mu, *J. Power Sources*, 2013, **240**, 381-389.
22. T. Palaniselvam, H. B. Aiyappa and S. Kurungot, *J. Mater. Chem.*, 2012, **22**, 23799-23805.
23. B. Chen, S. Xiang and G. Qian, *Acc. Chem. Res.*, 2010, **43**, 1115-1124.
24. H. Hayashi, A. P. Cote, H. Furukawa, M. O'Keeffe and O. M. Yaghi, *Nat. Mater.*, 2007, **6**, 501-506.
25. R. E. Morris and P. S. Wheatley, *Angew. Chem. Int. Ed.*, 2008, **47**, 4966-4981.
26. H.-L. Jiang, B. Liu, Y.-Q. Lan, K. Kuratani, T. Akita, H. Shioyama, F. Zong and Q. Xu, *J. Am. Chem. Soc.*, 2011, **133**, 11854-11857.
27. B. Liu, H. Shioyama, H. L. Jiang, X. B. Zhang and Q. Xu, *Carbon*, 2010, **48**, 456-463.
28. P. Song, Y. Q. Li, W. Li, B. He, J. Z. Yang and X. G. Li, *Int. J. Hydrogen Energy*, 2011, **36**, 10468-10473.
29. Y. Q. Li, L. Xie, Y. Li, J. Zheng and X. G. Li, *Chem.-Eur. J.*, 2009, **15**, 8951-8954.
30. E. Proietti, F. Jaouen, M. Lefevre, N. Larouche, J. Tian, J. Herranz and J.-P. Dodelet, *Nat. Commun.*, 2011, **2**, 416.
31. S. Q. Ma, G. A. Goenaga, A. V. Call and D. J. Liu, *Chem.-Eur. J.*, 2011, **17**, 2063-2067.
32. J. Tian, A. Morozan, M. T. Sougrati, M. Lefevre, R. Chenitz, J.-P. Dodelet, D. Jones and F. Jaouen, *Angew. Chem. Int. Ed.*, 2013, **52**, 6867-6870.
33. T. Palaniselvam, B. P. Biswal, R. Banerjee and S. Kurungot, *Chem.-Eur. J.*, 2013, **19**, 9335-9342.

34. D. Zhao, J.-L. Shui, L. R. Grabstanowicz, C. Chen, S. M. Commet, T. Xu, J. Lu and D.-J. Liu, *Adv. Mater.*, 2014, **26**, 1093-1097.
35. P. Zhang, F. Sun, Z. Xiang, Z. Shen, J. Yun and D. Cao, *Energy & Environ. Sci.*, 2013, **7**, 442-450.
36. S. Cao, T. D. Bennett, D. A. Keen, A. L. Goodwin and A. K. Cheetham, *Chem. Commun.*, 2012, **48**, 7805-7807.
37. D. Wang and D. S. Su, *Energy & Environ. Sci.*, 2013, **7**, 576-591.
38. S. Mao, Z. Wen, T. Huang, Y. Hou and J. Chen, *Energy & Environ. Sci.*, 2014, **7**, 609-616.
39. J. Wang, H. Qin, J. Liu, Z. Li, H. Wang, K. Yang, A. Li, Y. He and X. Yu, *J. Phys. Chem. C*, 2012, **116**, 20225-20229.
40. J. K. Dombrovskis, H. Y. Jeong, K. Fossum, O. Terasaki and A. E. C. Palmqvist, *Chem. Mater.*, 2013, **25**, 856-861.
41. U. I. Kramm, J. Herranz, N. Larouche, T. M. Arruda, M. Lefèvre, F. Jaouen, P. Bogdanoff, S. Fiechter, I. Abs-Wurmbach, S. Mukerjee and J.-P. Dodelet, *Phys. Chem. Chem. Phys.*, 2012, **14**, 11673.
42. F. Jaouen, E. Proietti, M. Lefevre, R. Chenitz, J. P. Dodelet, G. Wu, H. T. Chung, C. M. Johnston and P. Zelenay, *Energy & Environ. Sci.*, 2011, **4**, 114-130.
43. T. Sharifi, F. Nitze, H. R. Barzegar, C.-W. Tai, M. Mazurkiewicz, A. Malolepszy, L. Stobinski and T. Wagberg, *Carbon*, 2012, **50**, 3535-3541.
44. F. Nitze, B. M. Andersson and T. Wagberg, *Physica Status Solidi B-Basic Solid State Physics*, 2009, **246**, 2440-2443.
45. H. R. Byon, J. Suntivich and Y. Shao-Horn, *Chem. Mater.*, 2011, **23**, 3421-3428.
46. G. Wu, Z. W. Chen, K. Artyushkova, F. H. Garzon and P. Zelenay, in *Proton Exchange Membrane Fuel Cells 8, Pts 1 and 2*, eds. T. Fuller, K. Shinohara, V. Ramani, P. Shirvanian, H. Uchida, S. Cleghorn, M. Inaba, S. Mitsushima, P. Strasser, H. Nakagawa, H. A. Gasteiger, T. Zawodzinski and C. Lamy, Electrochemical Society Inc, Pennington, 2008, pp. 159-170.

ZIF-67, a MOF with N-coordinated Co atoms can assist the formation of active sites in the oxygen reduction catalyst by pyrolysis and acid leaching.